Pramana – J. Phys. (2021) 95:5
https://doi.org/10.1007/s12043-020-02029-1

Impact of metal oxide nanoparticles on unsteady stagnation point flow of the hybrid base fluid along a flat surface

AMIT KUMAR PANDEY[1], SOHITA RAJPUT[1], KRISHNENDU BHATTACHARYYA[1,*] and PRECIOUS SIBANDA[2]

[1]Department of Mathematics, Institute of Science, Banaras Hindu University, Varanasi 221 005, India
[2]School of Mathematics, Statistics and Computer Science, University of KwaZulu-Natal, Private Bag X01, Scottsville, Pietermaritzburg 3209, South Africa
*Corresponding author. E-mail: krish.math@yahoo.com, krishmath@bhu.ac.in

MS received 4 May 2020; revised 4 August 2020; accepted 19 August 2020

Abstract. This paper deals with a detailed investigation of the effects of various metal oxide nanoparticles on unsteady stagnation point flow of a hybrid base fluid impinging on a flat surface. The 'single-phase' nanofluid model, i.e., the Tiwari and Das model, is considered for the study. We consider water and ethylene glycol in 1:1 ratio as the base fluid and four different types of metal oxides, namely, CuO, TiO_2, ZnO and MgO as the nanoparticles. Using similarity transformations, the conservation equations are transformed into self-similar ordinary differential equations. Dual and unique similarity solutions are obtained for certain set of values of parameters. The analysis explores many important findings. Dual self-similar solutions exist up to a certain critical value of the decelerating unsteady parameter and the critical value is independent of the type of metal oxide nanoparticles considered. The strongest surface drag force is observed for the nanofluid with CuO nanoparticles, while the weakest is for the nanofluid with MgO nanoparticles. The heat transfer rate is highest for the nanofluid with CuO nanoparticles and lowest for the nanofluid with TiO_2 nanoparticles. Also, the boundary layer is thickest for the nanofluid with MgO nanoparticles.

Keywords. Metal oxide nanoparticles; hybrid base fluid; dual solutions; stability analysis; unsteady stagnation-point flow.

PACS Nos **47.15.Cb; 47.15.Fe; 47.61.−k**

1. Background of investigation

Nanotechnology is an exceptionally multifaceted area of study that has attracted research minds in various fields in science, engineering and technology to study its wide range of applications in different essential services and industries, such as, pharmaceutical medicine, electronics and agriculture, industrial chemical processes and many similar industries. An important achievement in the field of nanotechnology is the introduction of a nanofluid, which has gained attention of many researchers owing to growing demands for enhancing the rate of heat transfer. The concept of nanofluid was proposed by Choi [1] in 1995. Through his detailed and in-depth study, Choi suggested that nanofluids are extremely critical for optimising heat transfer rates. The accuracy of his results was corroborated experimentally by Lee *et al* [2] and Kang *et al* [3], who measured fluid thermal conductivity by the method of transient hot-wire. Their experiments confirm that the random movement of nanoparticles (NPs) enhances fluid thermal conductivity. These nanofluids are developed by diffusing NPs of the desired metals in a fluid which acts as the base. As of now, numerous NPs and base fluids have been explored by various researchers. The commonly used NPs are magnetic, polymeric and metallic NPs, carbon nanotubes, and many others. These are diffused in a base fluid, either water, oil, ethylene glycol, or in different combinations of these fluids. Various NPs in the metallic domain are alumina, copper, carbides, metal oxides, nitrides, etc.

Currently, there are two types of distinct nanofluid models, which can be utilised for studying the performance of a nanofluid, namely, the Buongiorno [4] model and Tiwari and Das [5] model. The model given by Tiwari and Das, which is commonly recognised as a 'single-phase' model, takes into account the effects of volume fractions of different NPs, whereas

Published online: 03 February 2021

Table 1. Thermophysical properties of metal oxides and water–ethylene glycol (1:1) hybrid base fluid.

Physical properties	Water–ethylene glycol (1:1)	Metal oxides			
		CuO	TiO_2	ZnO	MgO
ρ (kg/m^3)	1063.8	6320	4250	5700	3580
C_p (J/kg K)	3630	531.8	686.2	523	879
k (W/mK)	0.387	76.5	8.9538	25	30

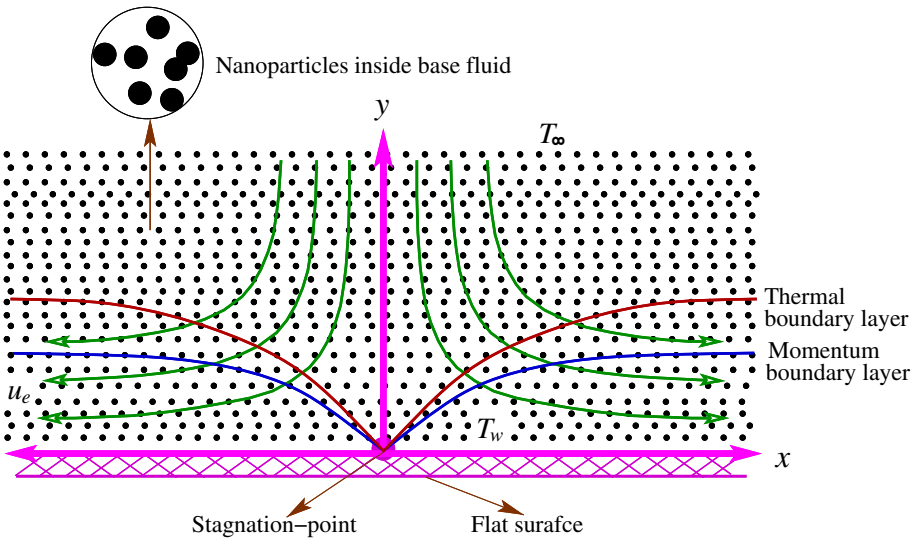

Figure 1. Physical sketch of the problem.

the Buongiorno model known as the 'two-phase' model considers both Brownian motion of the NPs and their thermophoresis effects. Studies by Ebrahimi *et al* [6] and Pang *et al* [7] revealed that the thermal characteristics of a nanofluid can be differently enhanced by diffusing different types of NPs, their volume fractions, sizes including diameters. They also showed that nanofluids are viable alternatives for any application which requires the optimisation of a heat transfer process. Hence, the creation of stable nanofluids was a landmark event in the area of heat transfer enhancement. This is imperative in many fields, e.g., energy saving processes, air conditioning and refrigeration systems, solar collectors and automotive industries. These applications of nanofluid are widely discussed in [8–12]. Considering the effects of Brownian motion, Eckert and Schmidt numbers, Sheikholeslami and Ganji [13] worked on the nanofluid flow subjected to the unsteady squeezing and transfer of heat between two infinite parallel plates with thermal radiation. In 2014, Malvandi and Ganji [14] investigated the convective transfer of heat in water–alumina nanofluid subjected to a magnetic field within a given channel. Their results suggested that the magnetic field affects the migration of NPs from the region of hot walls to the channel central region and also the velocity gradient near the wall. Ultimately, these factors have a huge impact on the rate of heat transfer and pressure drop. Similarly, Ahmed and Mustafa [15] investigated five distinct types of nanofluids in rotating flow past a sheet which is exponentially stretching. Their study showed that the maximum heat transfer was achieved with Al_2O_3–water nanofluid and the minimum with Ag–water nanofluid. Hosseinzadeh *et al* [16] discussed the effects of Brownian motion and thermophoretic force on MHD nanofluid flow between two parallel plates and Derakhshan *et al* [17] described heat and mass transfer in magnetic nanofluid flow between two parallel plates. To solve the first problem, three methods, namely, collocation method (CM), homotopy perturbation method (HPM) and finite element method (FEM) are used, whereas the latter one is solved by using Akbari–Ganji's method (AGM). Zangooee *et al* [18] reported the MHD nanofluid flow between two stretchable rotating disks with homogeneous–heterogeneous reactions. Hosseinzadeh *et al* [19] analysed the entropy generation in MHD nanofluid flow, where ethylene glycol is taken as the base fluid and carbon nanotubes are taken as nanoparticles. Some other important aspects of similar flow dynamics are explored by researchers [20–29] in recent years.

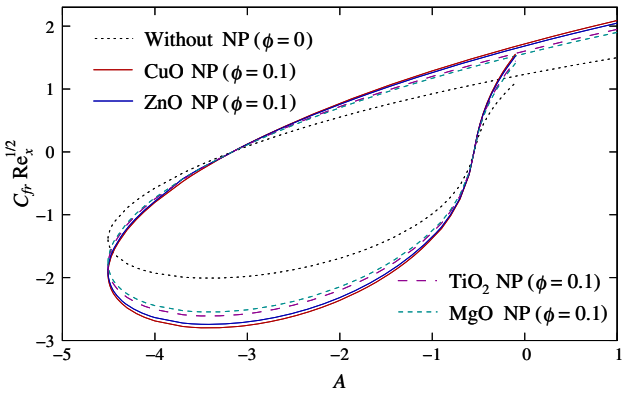

Figure 2. Skin-friction coefficient vs. A for the nanofluids with different types of metal oxide nanoparticles (NPs).

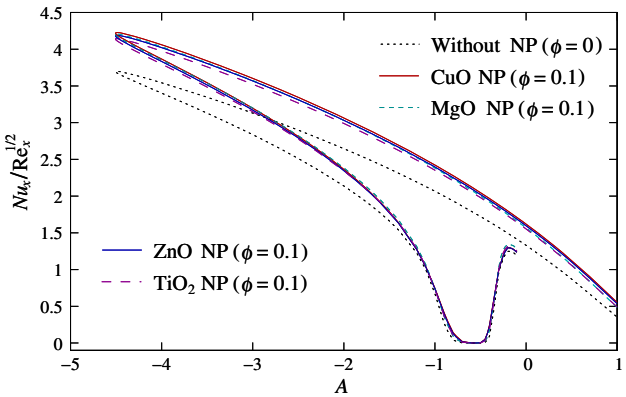

Figure 3. Nusselt number vs. A for the nanofluids with different types of metal oxide NPs.

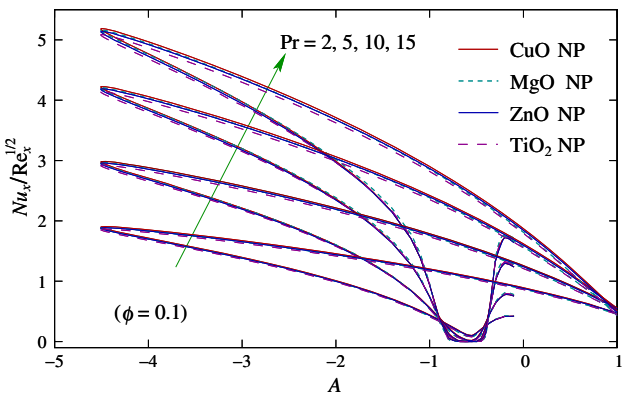

Figure 4. Nusselt number vs. A for different values of Pr of the nanofluids with various metal oxide NPs.

The stagnation point flow describes the motion of a fluid near a stagnation region. This type of flow occurs when the flow collides with a solid surface and the velocity of the fluid at the stagnation point becomes zero. This type of flow exists near the tip points of ships, submarines, aircrafts and rockets. The flow happens in a high-pressure situation near the stagnation point and can produce very high heat transfer when the nanofluid is considered. As a consequence, stagnation point flow of the nanofluid is hugely applicable in many engineering systems, such as heat exchanger, microelectronics cooling design, heat transfer in atmospheric re-entry, etc. Bachok *et al* [30] studied the stagnation point flow of copper–water nanofluid and heat transfer over a stretching/shrinking sheet. The transfer of heat near the stagnation point and an unsteady boundary layer near a shrinking or stretching sheet were investigated by Bhattacharyya [31]. Free convection of water-based nanofluid (containing Al_2O_3, Cu, TiO_2, Ag) past a vertical plate with thermal stratification was examined by Peddisetty [32]. In 2017, Ghadikolaei [33] evaluated a hybrid TiO_2–Cu/water nanofluid stagnation point flow over a stretching sheet by taking into account the induced magnetic field. The flow of a hybrid TiO_2–MWCNTs–water nanofluid was investigated and studied experimentally by Akhgar and Toghraie [34]. They utilised two models and established that thermal conductivity is augmented by 38.7%. Further, Esfahani and Toghraie [35] studied water/silica–ethylene glycol and suggested that optimum thermal conductivity occurred when the NP volume fraction was 5%. The flow of an unsteady nanofluid over a sheet which is exponentially shrinking and with thermal radiation was examined by Uddin *et al* [36]. Sheikholeslami and Ganji [37] studied CuO–H_2O nanofluid flow with forced convection subjected to a magnetic field. Gholinia *et al* [38] analysed mixed convection stagnation point flow of the nanofluid on a vertical permeable circular cylinder with silver and copper nanoparticles and obtained numerical solutions using a Maple package. Ghadikolaei *et al* [39] examined MHD stagnation flow of Eyring–Powell nanofluid on cylindrical stretching surface with nonlinear thermal radiation and chemical reaction.

The main aim of this work is to analyse the impact of various metal oxide NPs on the unsteady stagnation point flow of a nanofluid along a flat surface. Water and ethylene glycol in 1:1 ratio is taken as the hybrid base fluid and four different metal oxide NPs, namely, copper oxide (CuO), titanium oxide (TiO_2), magnesium oxide (ZnO) and zinc oxide (MgO), are considered separately. Actually, metal oxide nanoparticles display quite different physical and chemical properties for their smaller size and also those are very stable systems with well-defined crystallographic structures. Here, the nanofluid model proposed by Das and Tiwari is used to study the effect of different metal oxide NPs on various flow and heat transfer properties. The governing system is transformed into ODEs, which are numerically solved using the shooting method. The obtained numerical results are presented graphically for various parameters and the

impacts of changes of those parameters on fluid properties are discussed in detail.

2. Mathematical formulation

Consider the unsteady boundary layer flow near a stagnation point in a hybrid nanofluid along a flat surface. The external flow velocity is assumed to be a variable in the form $u_e(x,t) = ax\,(1-ct)^{-1}$, where a and c are constants. The wall temperature T_w is assumed to be constant. The temperature at free stream, T_∞ is also constant. Under these assumptions along with the boundary layer structure, the conservation equations are [31,40]

$$\frac{\partial u}{\partial x}+\frac{\partial v}{\partial y}=0, \tag{1}$$

$$\frac{\partial u}{\partial t}+u\frac{\partial u}{\partial x}+v\frac{\partial u}{\partial y}=\frac{\partial u_e}{\partial t}+u_e\frac{\partial u_e}{\partial x}+\upsilon_{nf}\frac{\partial^2 u}{\partial y^2}, \tag{2}$$

$$\frac{\partial T}{\partial t}+u\frac{\partial T}{\partial x}+v\frac{\partial T}{\partial y}=\frac{\kappa_{nf}}{(\rho c_p)_{nf}}\frac{\partial^2 T}{\partial y^2}. \tag{3}$$

The appropriate boundary conditions are

$$\left.\begin{aligned} &t<0:\ u=0,\ v=0,\ T=T_w \text{ for any } x,\ y,\\ &t\geq 0:\ u=0,\ v=0,\ T=T_w \text{ at } y=0,\\ &\quad u\to u_e(x,t),\ T\to T_\infty \text{ as } y\to\infty, \end{aligned}\right\} \tag{4}$$

where u and v are components of velocity along x- and y-axes, respectively, T is the temperature of the nanofluid, $\upsilon_{nf}(=\mu_{nf}/\rho_{nf})$ is the kinematic viscosity of the nanofluid, $(\rho c_p)_{nf}$ is the heat capacity of the nanofluid, κ_{nf} is the thermal conductivity of the nanofluid, μ_{nf} is the viscosity of the nanofluid and ρ_{nf} is the density of the nanofluid, which are defined as [32]

$$\left.\begin{aligned} &\rho_{nf}=(1-\phi)\rho_f+\phi\rho_s,\\ &\mu_{nf}=\frac{\mu_f}{(1-\phi)^{2.5}},\ \upsilon_{nf}=\frac{\mu_{nf}}{\rho_{nf}},\\ &(\rho c_p)_{nf}=(1-\phi)(\rho c_p)_f+\phi(\rho c_p)_s,\\ &\frac{\kappa_{nf}}{\kappa_f}=\frac{\kappa_s+2\kappa_f-2\phi(\kappa_f-\kappa_s)}{\kappa_s+2\kappa_f+\phi(\kappa_f-\kappa_s)}. \end{aligned}\right\} \tag{5}$$

Here, ϕ is the NP volume fraction, κ_f and κ_s are thermal conductivities of the fluid and solid particles, respectively, ρ_f and ρ_s are densities of the fluid and solid particles, respectively and μ_f is the viscosity of the base fluid. Here, four types of metal oxide NPs; CuO, TiO_2, ZnO and MgO are considered and thermal properties of these NPs are given in table 1. A schematic sketch of the problem is presented in figure 1.

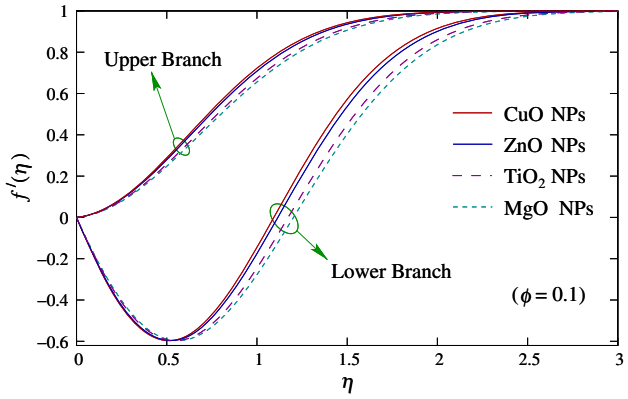

Figure 5. Velocity profiles for the nanofluids with different metal oxide NPs when $A=-3$.

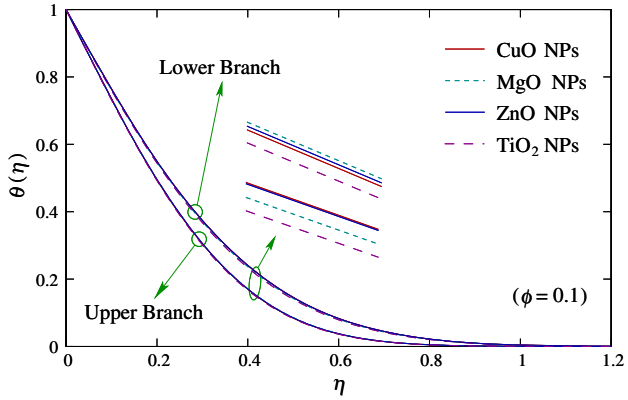

Figure 6. Temperature profiles for the nanofluids with different metal oxide NPs when $A=-3$.

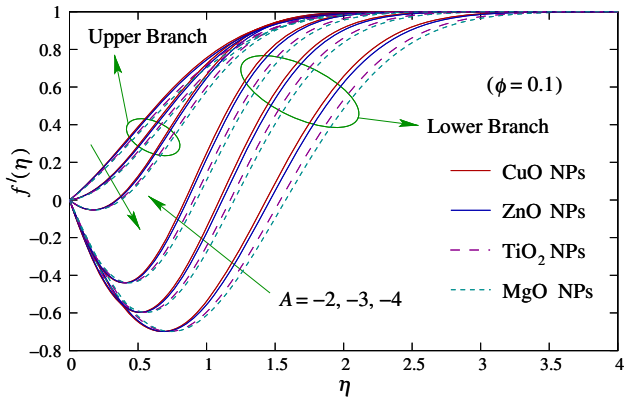

Figure 7. Velocity profiles for different values of A of the nanofluids with various metal oxide NPs.

The following similarity transformations are adopted to reduce PDEs to ODEs:

$$\eta=\sqrt{\frac{u_e}{\upsilon_f x}}\,y,\quad \psi=\sqrt{u_e x\upsilon_f}\,f(\eta),$$
$$T=T_\infty+(T_w-T_\infty)\theta(\eta), \tag{6}$$

where η is a similarity variable, $\upsilon_f (= \mu_f/\rho_f)$ is the kinematic viscosity of the base fluid and ψ is the stream function defined as

$$u = \frac{\partial \psi}{\partial y} \text{ and } v = -\frac{\partial \psi}{\partial x},$$

for which the equation of continuity (1) is identically satisfied. In view of relation (6), we have the following transformed self-similar ODEs:

$$\frac{1}{\phi_1} f''' + f f'' - f'^2 + 1 - A\left(f' + \frac{1}{2}\eta f'' - 1\right) = 0, \tag{7}$$

$$\frac{\kappa_{nf}/\kappa_f}{\phi_2}\theta'' + \Pr\ f\theta' - \frac{A\,\Pr}{2}\eta\theta' = 0, \tag{8}$$

where $A = c/a$ is the unsteady parameter, $\Pr = \upsilon_f/[\kappa_f(\rho c_p)_f]$ is the Prandtl number and ϕ_1 and ϕ_2 are given as

$$\phi_1 = (1-\phi)^{2.5}\left(1 - \phi + \phi\frac{\rho_s}{\rho_f}\right)$$

and

$$\phi_2 = \left[1 - \phi + \phi\frac{(\rho c_p)_s}{(\rho c_p)_f}\right].$$

The transformed boundary conditions in (4) are

$$\left.\begin{array}{l} f(0) = 0,\ \ f'(0) = 0,\ \ \theta(0) = 1, \\ f'(\infty) = 1,\ \ \theta(\infty) = 0. \end{array}\right\} \tag{9}$$

The skin friction and Nusselt number are given as

$$C_f = \frac{\tau_w}{\rho_f u_e^2},\ \ Nu_x = \frac{x}{\kappa_f}\frac{q_w}{(T_w - T_\infty)}, \tag{10}$$

where τ_w, the wall shear stress and q_w, the heat transfer rate at the surface are defined as

$$\tau_w = \mu_{nf}\left(\frac{\partial u}{\partial y}\right)_{y=0},\ \ q_w = -\kappa_{nf}\left(\frac{\partial T}{\partial y}\right)_{y=0.} \tag{11}$$

Inserting (6) into (10) and using (11), we get

$$C_f \mathrm{Re}_x^{1/2} = \frac{1}{(1-\varphi)^{2.5}} f''(0),\ \ Nu_x/\mathrm{Re}_x^{1/2} = -\frac{\kappa_{nf}}{\kappa_f}\theta'(0), \tag{12}$$

where $\mathrm{Re}_x = u_e x/\upsilon_f$ is the local Reynolds number.

3. Solution methodology and its validation

The transformed nonlinear coupled self-similar higher-order ODEs (7)–(8) with (9) form a boundary value problem (BVP) and it is solved using the classical shooting method after converting it to an initial value problem (IVP) consisting of a system of first-order ODEs given as

$$\left.\begin{array}{l} y_1' = y_2, \\ y_2' = y_3, \\ y_3' = \phi_1\left[y_2^2 - y_1 y_3 - 1 + A(y_2 + \eta y_3/2 - 1)\right], \end{array}\right\} \tag{13}$$

$$\left.\begin{array}{l} y_4' = y_5, \\ y_5' = \dfrac{\phi_2\,\Pr}{\kappa_{nf}/\kappa_f}\left[\dfrac{A}{2}\eta y_5 - y_1 y_5\right] \end{array}\right\} \tag{14}$$

with

$$y_1(0) = 0,\ \ y_2(0) = 0,\ \ y_4(0) = 1, \tag{15}$$

where $y_1(\eta) = f(\eta)$ and $y_4(\eta) = \theta(\eta)$.

Here, we have to choose a fixed finite value of $\eta \to \infty$, say $\eta_\infty (= 15)$. In addition, to obtain the solutions, we need $y_3(0)$ and $y_5(0)$, and assuming a series of guess values of $y_3(0)$ and $y_5(0)$ the integration is carried out by the fourth-order R–K method. In each iteration, solutions are obtained which are compared with $y_2(\eta_\infty) = 1,\ \ y_4(\eta_\infty) = 0$. Emphasis is given to obtain solutions with asymptotic convergence to boundary conditions by maintaining the desired accuracy level, 10^{-5} during computations.

In addition, to ensure the accuracy of the adopted numerical scheme, a comparison of computed values (dual) of $f''(0)$ for different values of A for $\phi = 0.1$ taking TiO_2 as the nanoparticles and H_2O as the base fluid with the results by Bachok *et al* [40] is made and those two sets of results appear to be in excellent agreement, which confirms the accuracy of the numerical scheme as well as all developed results (table 2).

Table 2. Comparison of the values of $f'(0)$ for different values of A with $\phi = 0.1$ taking TiO_2 as the nanoparticles and H_2O as the base fluid.

A	Bachok *et al* [40]	Present study
1	1.5128	1.512797
−1	0.9320[−0.9945]	0.931990[−0.994517]
−2	0.5585[−1.7088]	0.558471[−1.708830]
−3	0.0898[−1.9981]	0.089776[−1.998114]
−4	−0.5806[−1.9461]	−0.580639[−1.946119]

Values within [ ] are for lower branch solutions.

4. Stability analysis

In the present work, dual solutions exist in specific ranges of a specified parameter. To determine the instability of solutions, a stability analysis is performed following Weidman *et al* [41] and Bakar *et al* [42]. A new dimensionless similarity variable τ is introduced

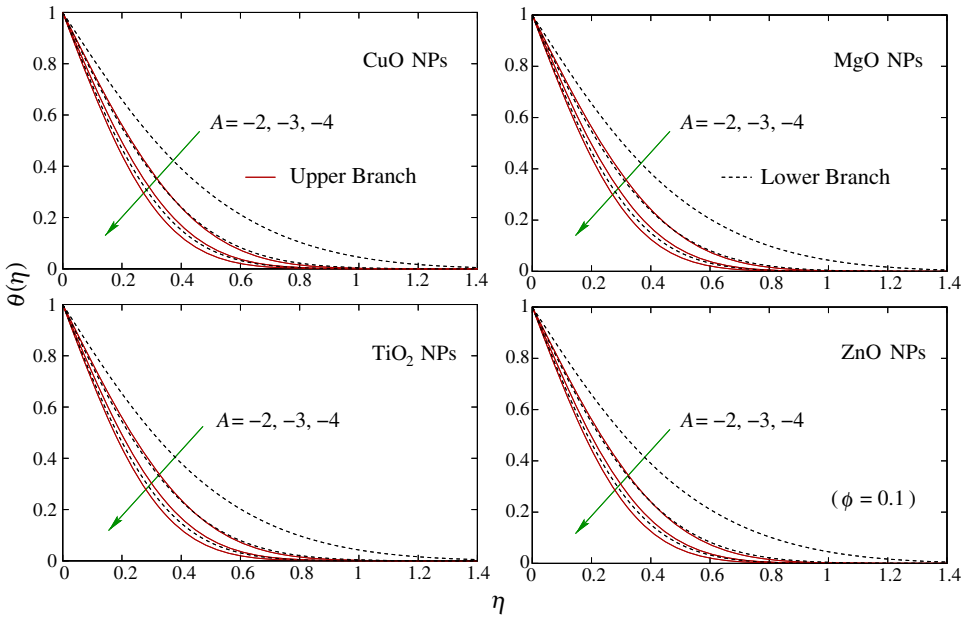

Figure 8. Temperature profiles for different values of A of the nanofluids with various metal oxide NPs.

and the unsteady similarity solutions are taken as

$$\psi = \sqrt{x\upsilon_f u_e}F(\eta,\tau),\ \ T=T_\infty+(T_w-T_\infty)\Phi(\eta,\tau),$$
$$\eta = \sqrt{\frac{u_e}{x\upsilon_f}}y,\ \ \tau = \frac{u_e t}{x}. \tag{16}$$

Substituting eq. (16) into (2) and (3) with (4) we finally get

$$\frac{1}{\phi_1}\frac{\partial^3 F}{\partial\eta^3} + F\frac{\partial^2 F}{\partial\eta^2} - \left(\frac{\partial F}{\partial\eta}\right)^2 + 1 - A\left(\frac{\partial F}{\partial\eta} + \frac{\eta}{2}\frac{\partial^2 F}{\partial\eta^2} - 1 + \tau\frac{\partial^2 F}{\partial\tau\partial\eta}\right) - \frac{\partial^2 F}{\partial\tau\partial\eta} = 0, \tag{17}$$

$$\frac{\kappa_{nf}/\kappa_f}{\phi_2}\frac{\partial^2\Phi}{\partial\eta^2} + \Pr\left(F\frac{\partial\Phi}{\partial\eta} - \frac{\partial\Phi}{\partial\tau}\right) - A\Pr\left(\frac{\eta}{2}\frac{\partial\Phi}{\partial\eta} + \tau\frac{\partial\Phi}{\partial\tau}\right) = 0, \tag{18}$$

along with the boundary conditions

$$\left.\begin{aligned} &F(0,\tau)=0,\ \ F'(0,\tau)=0,\ \ \Phi(0,\tau)=1,\\ &F'(\eta,\tau)\to 1,\ \ \Phi(\eta,\tau)\to 0 \text{ as } \eta\to\infty. \end{aligned}\right\} \tag{19}$$

In order to test the stability of solutions $f(\eta), \theta(\eta)$ satisfying the BVP (7)–(9), we introduce (Weidman *et al* [41])

$$\left.\begin{aligned} F(\eta,\tau) &= f(\eta) + \mathrm{e}^{-\gamma\tau}f^*(\eta,\tau),\\ \Phi(\eta,\tau) &= \theta(\eta) + \mathrm{e}^{-\gamma\tau}\theta^*(\eta,\tau), \end{aligned}\right\} \tag{20}$$

where $f^*(\eta,\tau),\ \theta^*(\eta,\tau)$ are disturbances to solutions $f(\eta),\ \theta(\eta)$ and are assumed very small compared to the solutions and γ is the rate of disturbance. Using (20) in (17)–(19) and linearising we have

$$\frac{1}{\phi_1}\frac{\partial^3 f^*}{\partial\eta^3} + f\frac{\partial^2 f^*}{\partial\eta^2} + f^*\frac{\mathrm{d}^2 f}{\mathrm{d}\eta^2} - 2\frac{\mathrm{d}f}{\mathrm{d}\eta}\frac{\partial f^*}{\partial\eta} - A\left(\frac{\partial f^*}{\partial\eta} + \frac{\eta}{2}\frac{\partial^2 f^*}{\partial\eta^2} + \tau\frac{\partial^2 f^*}{\partial\tau\partial\eta} - \gamma\tau\frac{\partial f^*}{\partial\eta}\right) - \frac{\partial^2 f^*}{\partial\tau\partial\eta} + \gamma\frac{\partial f^*}{\partial\eta} = 0 \tag{21}$$

$$\frac{\kappa_{nf}/\kappa_f}{\phi_2}\frac{\partial^2\theta^*}{\partial\eta^2} + \Pr\left(f\frac{\partial\theta^*}{\partial\eta} + f^*\frac{\mathrm{d}\theta}{\mathrm{d}\eta} - \frac{\partial\theta^*}{\partial\tau} + \gamma\theta^*\right) - A\Pr\left(\frac{\eta}{2}\frac{\partial\theta^*}{\partial\eta} + \tau\frac{\partial\theta^*}{\partial\tau} - \tau\gamma\theta^*\right) = 0 \tag{22}$$

subject to boundary conditions

$$\left.\begin{aligned} &f^*(0,\tau)=0,\ \ \frac{\partial f^*}{\partial\eta}(0,\tau)=0,\ \ \theta^*(0,\tau)=0,\\ &\frac{\partial f^*}{\partial\eta}(\infty,\tau)\to 0,\ \theta^*(\infty,\tau)\to 0. \end{aligned}\right\} \tag{23}$$

Now, setting $\tau = 0$ and putting $f^*(\eta,\tau) = f_0^*(\eta)$ and $\theta^*(\eta,\tau) = \theta_0^*(\eta)$ ($f_0^*(\eta)$ and $\theta_0^*(\eta)$ are the initial disturbances to the solutions) in eqs (21)–(23) we get

$$\frac{1}{\phi_1}\frac{\mathrm{d}^3 f_0^*}{\mathrm{d}\eta^3} + f\frac{\mathrm{d}^2 f_0^*}{\mathrm{d}\eta^2} + f_0^*\frac{\mathrm{d}^2 f}{\mathrm{d}\eta^2} - 2\frac{\mathrm{d}f}{\mathrm{d}\eta}\frac{\mathrm{d}f_0^*}{\mathrm{d}\eta}$$

$$-A\left(\frac{\mathrm{d}f_0^*}{\mathrm{d}\eta}+\frac{\eta}{2}\frac{\mathrm{d}^2 f_0^*}{\mathrm{d}\eta^2}\right)+\gamma\frac{\mathrm{d}f_0^*}{\mathrm{d}\eta}=0 \tag{24}$$

$$\frac{\kappa_{nf}/\kappa_f}{\phi_2}\frac{\mathrm{d}^2\theta_0^*}{\mathrm{d}\eta^2}+\mathrm{Pr}\left(f\frac{\mathrm{d}\theta_0^*}{\mathrm{d}\eta}+f_0^*\frac{\mathrm{d}\theta}{\mathrm{d}\eta}+\gamma\theta_0^*\right)-\frac{\eta A\,\mathrm{Pr}}{2}\frac{\mathrm{d}\theta_0^*}{\mathrm{d}\eta}=0 \tag{25}$$

along with the boundary condition

$$\left.\begin{aligned} &f_0^*(0)=0,\ \frac{\mathrm{d}f_0^*}{\mathrm{d}\eta}(0)=0,\ \theta_0^*(0)=0,\\ &\frac{\mathrm{d}f_0^*}{\mathrm{d}\eta}(\infty)\to 0,\ \theta_0^*(\infty)\to 0. \end{aligned}\right\} \tag{26}$$

This gives an eigenvalue problem with γ an unknown eigenvalue. An infinite set of eigenvalues $\gamma_1 < \gamma_2 < \gamma_3 < \cdots$ will be generated on solving the eigenvalue problems (24)–(26). The sign of the smallest eigenvalue γ_1 determines the stability of the solutions $f(\eta)$ and $\theta(\eta)$. If γ_1 is positive, this indicates an initial decay of disturbances and the solutions are stable and if γ_1 is negative then this is a clear indication of the initial growth of disturbances and hence the solutions are unstable.

5. Results and discussion

The numerical solutions of the transformed self-similar ODEs are computed for various values of involved parameters, namely, the unsteady parameter (A), Prandtl number (Pr) and four types of metal oxide NPs; CuO, TiO_2, ZnO and MgO. Computed results reveal many important findings on the flow characteristics along with impacts of various metal oxide NPs and those are presented in figures 2–8. Figures 2–4 confirm the existence of dual solutions for certain cases of decelerating unsteady flow. Dual solutions are found for $A < 0$ and up to a critical value, A_c (say) and no solution exists when $A < A_c$. It is worth noting that the nature of the metal oxide NPs does not affect the critical value, A_c. For all cases with and without NP, the value of A_c is -4.50664. This implies that for $-4.50664 \leq A < 0$ dual solutions exist and for $A \geq 0$ a unique solution is obtained. The values of skin-friction coefficient are plotted in figure 2 as a function of the unsteady parameter A for different metal oxide NPs and for no NPs. It is found that for the case without any NP ($\phi = 0$), the skin-friction coefficient value is the lowest at the upper branch for small magnitudes of decelerating ($A < 0$) and any value of accelerating ($A > 0$) unsteady parameter and it is the largest at lower branch for all values of unsteady parameter except near the zero value. Similarly, in the study with four metal oxide NPs ($\phi = 0.1$ for all), the value of skin friction coefficient, and consequently the surface drag force, is maximum for a nanofluid with CuO NPs among all four at upper branch and it is minimum at lower branch (values of A are as specified above). Further, skin-friction coefficient values for nanofluids containing ZnO, TiO_2, MgO NPs decrease in the upper branch with small negative values of the unsteady parameter and vice versa at the lower branch. It means that the drag force for the nanofluid with ZnO NPs is larger than that for a nanofluid with TiO_2 NPs and the drag force for a nanofluid with TiO_2 NP is slightly higher than that of a nanofluid with MgO NPs corresponding to the upper branch and the trend is opposite at the lower branch. The density ratio of the base fluid and the nanoparticle for the nanofluid with CuO NPs is larger than all other types and due to this reason more surface drag force is generated, whereas for the nanofluid with MgO NPs that ratio is the least. Figure 3 shows the variation of the Nusselt number with A for the nanofluids with different metal oxide NPs. The heat transfer rate is the lowest for both solution branches when there is no NP ($\phi = 0$). Similarly, out of the four metal oxide NPs with volume fraction, $\phi = 0.1$, heat transfer is the highest for the nanofluid with CuO NPs at the upper and lower branches (except for a few values of A). Also, heat transfer rate for a nanofluid with MgO NPs is higher than for a nanofluid with ZnO NPs for both branches, i.e., upper and lower. The heat transfer rate for a nanofluid with TiO_2 NPs is minimum among all four types of oxide NPs. The Nusselt number as a function of A for different Prandtl numbers Pr is given in figure 4. As expected, the heat transfer rate increases with Pr for all nanofluids in both branches of solution. Pr varies inversely with thermal conductivity, and so it is evident that the heat transfer rate grows with Pr.

The dual velocity profiles for the nanofluids with different metal oxides are shown in figure 5 with the volume fraction value, $\phi = 0.1$. The fluid velocity for the nanofluid with CuO NPs has the highest velocity in both branches, while the nanofluid with MgO NPs has the minimum fluid velocity. The ascending order of the boundary layer thickness of the nanofluid is as follows: nanofluid with CuO NPs < ZnO NPs < TiO_2 NPs < MgO NPs. The drag force at the surface for the nanofluid with CuO NPs is maximum, which is the cause for the thinnest boundary layer thickness in this case and on the other hand, the drag force is minimum for the nanofluid with MgO NPs. The corresponding temperature profiles are presented in figure 6 for different nanofluids. The temperature of the nanofluid with CuO NPs is the highest for the upper branch and for the lower branch, the maximum is obtained for the nanofluid with MgO NPs. The nanofluid temperature is the lowest for the nanofluid

Table 3. Smallest eigenvalue, γ_1 for some values of A with $\phi = 0.1$ for nanofluids with different metal oxide NPs.

	γ_1 for nanofluid with			
A	CuO NPs	TiO_2 NPs	ZnO NPs	MgO NPs
1	3.501705	3.512071	3.504169	3.517162
0.5	3.273219	3.275282	3.273699	3.276643
0	3.062807	3.063082	3.062812	3.063290
−1	2.645136 [−1.926717]	2.645113 [−1.927208]	2.645030 [−1.926797]	2.645103 [−1.927452]
−2	2.198791 [−1.812429]	2.198807 [−1.812409]	2.198763 [−1.812419]	2.198720 [−1.812375]
−3	1.678263 [−1.487008]	1.678258 [−1.486921]	1.678250 [−1.486918]	1.678324 [−1.486945]
−4	0.955334 [−0.900342]	0.955403 [−0.900349]	0.955403 [−0.900339]	0.955323 [−0.900324]
−4.3	0.604692 [−0.583373]	0.604837 [−0.583504]	0.604792 [−0.583448]	0.604754 [−0.583316]
−4.5	0.106612 [−0.106453]	0.106982 [−0.106453]	0.106489 [−0.106391]	0.106752 [−0.106158]
−4.506	0.032394 [−0.032390]	0.032474 [−0.032176]	0.032925 [−0.032396]	0.032856 [−0.032320]

Values within [ ] are for lower branch solutions.

with TiO_2 NPs. The velocity profiles of the nanofluids with various metal oxide NPs for a set of values of decelerating unsteady parameter $A(= -2, -3, -4)$ are depicted in figure 7. The flow velocity decreases (increases) with increasing magnitude of decelerating A for upper (lower) branch solution. In figure 8, the temperature profiles for the same set of values of A for all four nanofluids are shown. The temperature and thermal boundary layer thickness reduce with the magnitude of the decelerating unsteady parameter A. The thickness of the boundary layer for the upper branch is comparatively thin between the two branches.

We have performed a stability analysis and solved the eigenvalue problem. The smallest eigenvalues γ_1 are given in table 3 for the upper and lower branch solutions ($A < 0$) and unique solution ($A \geq 0$). The smallest eigenvalues for the upper branch solution and unique solution are positive, while for the lower branch solution it is negative and the total statistic is the same for each nanofluid (with different metal oxide NPs). The immediate conclusion is that the upper branch and unique solutions are stable, while the lower branch solution is unstable. In our opinion, the stability or instability of the solutions does not affect its physical existence in experiments.

6. Conclusions

The problem associated with an unsteady stagnation-point flow of a hybrid base fluid containing various metal oxide NPs has been modelled and investigated numerically. The problem is transformed into a BVP containing two coupled self-similar ODEs. Dual and unique similarity solutions of the problem have been obtained for certain values for involved parameters. From the analysis presented above, the following conclusions can be drawn:

a) Dual solutions were obtained when $A_c \leq A < 0$; no solution exists for $A < A_c(= -4.50664)$ for all nanofluids.
b) The skin-friction coefficient, i.e., the surface drag force is the highest for the nanofluid composed of CuO NPs at the upper branch and lowest at the lower branch.
c) The Nusselt number and hence the heat transfer rate for the nanofluid with CuO NPs is maximum and it is minimum for a nanofluid with TiO_2 NPs.
d) The heat transfer rate increases with increasing Pr for all types of nanofluids.
e) The boundary layer is thickest(/thinnest) for a nanofluid with MgO(/CuO) NPs.
f) The fluid temperature inside the boundary layer is the highest for the nanofluid with CuO(/MgO) NPs at the upper(/lower) branch, whereas for the nanofluid with TiO_2 NPs it is the lowest.
g) The fluid velocity reduces(/enhances) with increasing magnitude of the decelerating unsteady parameter A for the upper(/lower) branch solution.

Acknowledgements

The works of A K Pandey (09/013(0742)/2018-EMR-I) and S Rajput (09/013(0843)/2018-EMR-I) are supported by the Council of Scientific and Industrial Research, New Delhi, Ministry of Human Resources Development of India Grant.

References

[1] S U S Choi, *Developments and applications of non-Newtonian flows* edited by D A Siginer and H P Wang (ASME, New York, 1995) Vol. 66, pp. 99–105

[2] S Lee, S U S Choi, S Li and J A Eastman, *ASME J. Heat Transf.* **121**, 280 (1999)
[3] H U Kang, S H Kim and J M Oh, *Exp. Heat Transf.* **19**, 181 (2006)
[4] J Buongiorno, *ASME J. Heat Transf.* **128**, 240 (2006)
[5] R K Tiwari and M K Das, *Int. J. Heat Mass Transf.* **50**, 2002 (2007)
[6] A Ebrahimi, F Rikhtegar, A Sabaghan and E Roohi, *Energy* **101**, 190 (2006)
[7] C Pang, J Y Jung and Y T Kang, *Int. J. Heat Mass Transf.* **72**, 392 (2014)
[8] E Firouzfar, M Soltanieh, S H Noie and S H Saidi, *Appl. Therm. Eng.* **31**, 1543 (2011)
[9] E C Wang and A Z Wang, *Integr. Biol. (Camb.)* **6**, 9 (2014)
[10] M S Patil, S C Kin, J-H Seo and M-Y Lee, *Energies* **9**, 22 (2016)
[11] N A Che Sidik, N G Y Cheong and A Fazeli, *Appl. Mech. Mater.* **695**, 539 (2015)
[12] E Abu-Nada and H F Oztop, *Numer. Heat Transf. Part A: Appl.* **59**, 403 (2011)
[13] M Sheikholeslami and D D Ganji, *J. Braz. Soc. Mech. Sci. Eng.* **37**, 895 (2015)
[14] A Malvandi and D D Ganji, *J. Magn. Magn. Mater.* **362**, 172 (2014)
[15] R Ahmed and M Mustafa, *J. Mol. Liq.* **220**, 635 (2016)
[16] Kh Hosseinzadeh, A J Amiri, S S Ardahaie and D D Ganji, *Case Stud. Therm. Eng.* **10**, 595 (2017)
[17] R Derakhshan, A Shojaei, Kh Hosseinzadeh, M Nimafar and D D Ganji, *Case Stud. Therm. Eng.* **14**, 100439 (2019)
[18] M R Zangooee, Kh Hosseinzadeh and D D Ganji, *Case Stud. Therm. Eng.* **14**, 100460 (2019)
[19] Kh Hosseinzadeh, A Asadi, A R Mogharrebi, J Khalesi, S Mousavisani and D D Ganji, *Case Stud. Therm. Eng.* **14**, 100482 (2019)
[20] Kh Hosseinzadeh, M Gholinia, B Jafari, A Ghanbarpour, H Olfian and D D Ganji, *Heat Transf. Asian Res.* **48**(**2**), 744 (2019)
[21] M Gholinia, Kh Hosseinzadeh, H Mehrzadi, D D Ganji and A A Ranjbar, *Case Stud. Therm. Eng.* **13**, 100356 (2019)
[22] M Khan, M Irfan and W A Khan, *Pramana – J. Phys.* **92**: 17 (2019)
[23] S Ghosh and S Mukhopadhyay, *Pramana – J. Phys.* **92**: 93 (2019)
[24] A Shojaei, A J Amiri, S S Ardahaie, Kh Hosseinzadeh and D D Ganji, *Case Stud. Therm. Eng.* **13**, 100384 (2019)
[25] M I Khan, S Qayyum, S Farooq, T Hayat and A Alsaedi, *Pramana – J. Phys.* **93**: 62 (2019)
[26] Kh Hosseinzadeh, A R Mogharrebi, A Asadi, M Paikar and D D Ganji, *J. Mol. Liq.* **300**, 112347 (2020)
[27] S Ghosh and S Mukhopadhyay, *Pramana – J. Phys.* **94**: 61 (2020)
[28] A K Gautam, A K Verma, K Bhattacharyya and A Banerjee, *Pramana – J. Phys.* **94**: 108 (2020)
[29] Kh Hosseinzadeh, A Asadi, A R Mogharrebi, M E Azari and D D Ganji, *J Therm. Anal. Calorim.* (2020), https://doi.org/10.1007/s10973-020-09347-x
[30] N Bachok, A Ishak and I Pop, *Boundary Value Prob.* **39**, 13 (2013)
[31] K Bhattacharyya, *Ain Shams Eng. J.* **4**, 259 (2013)
[32] N C Peddisetty, *Pramana – J. Phys.* **87**: 62 (2016)
[33] S S Ghadikolaei, M Yassari, H Sadeghi, Kh Hosseinzadeh and D D Ganji, *Powder Technol.* **322**, 428 (2017)
[34] A Akhgar and D Toghraie, *Powder Technol.* **338**, 806 (2018)
[35] M A Esfahani and D Toghraie, *J. Mol. Liq.* **232**, 105 (2017)
[36] M S Uddin, A Zaib and K Bhattacharyya, *J. Appl. Mech. Tech. Phys.* **58**, 670 (2017)
[37] M Sheikholeslami and D D Ganji, *Int. J. Hydrogen Energy* **42**, 2748 (2017)
[38] M Gholinia, S Gholinia, Kh Hosseinzadeh and D D Ganji, *Res. Phys.* **9**, 1525 (2018)
[39] S S Ghadikolaei, Kh Hosseinzadeh and D D Ganji, *World J. Eng.* **16**(**1**), 51 (2019)
[40] N Bachok, A Ishak and I Pop, *Int. J. Heat Mass Transf.* **55**, 6499 (2012)
[41] P D Weidman, D G Kubitschek and A M J Davis, *Int. J. Eng. Sci.* **44**, 730 (2006)
[42] S A Bakar, N M Arifin, F M Ali, N Bachok and R Nazar, *J. Phys. Conf. Ser.* **890**, 012041 (2017)